Available online at www.sciencedirect.com
SCIENCE DIRECT®
International Journal of Heat and Mass Transfer 49 (2006) 4082–4094
International Journal of HEAT and MASS TRANSFER
www.elsevier.com/locate/ijhmt

New flow boiling heat transfer model and flow pattern map for carbon dioxide evaporating inside horizontal tubes

Lixin Cheng [a,b], Gherhardt Ribatski [a], Leszek Wojtan [a], John R. Thome [a,*]

[a] *Laboratory of Heat and Mass Transfer (LTCM), Faculty of Engineering Science (STI), École Polytechnique Fédérale de Lausanne (EPFL), CH-1015 Lausanne, Switzerland*

[b] *Institute of Process Engineering, University of Hannover, Callinstraße 36, 30167 Hannover, Germany*

Received 8 June 2005; received in revised form 24 March 2006
Available online 5 June 2006

Abstract

A new flow boiling heat transfer model and a new flow pattern map based on the flow boiling heat transfer mechanisms for horizontal tubes have been developed specifically for CO_2. Firstly, a nucleate boiling heat transfer correlation incorporating the effects of reduced pressure and heat flux at low vapor qualities has been proposed for CO_2. Secondly, a nucleate boiling heat transfer suppression factor correlation incorporating liquid film thickness and tube diameters has been proposed based on the flow boiling heat transfer mechanisms so as to capture the trends in the flow boiling heat transfer data. In addition, a dryout inception correlation has been developed. Accordingly, the heat transfer correlation in the dryout region has been modified. In the new flow pattern map, an intermittent flow to annular flow transition criterion and an annular flow to dryout region transition criterion have been proposed based on the changes in the flow boiling heat transfer trends. The flow boiling heat transfer model predicts 75.5% of all the CO_2 database within ±30%. The flow boiling heat transfer model and the flow pattern map are applicable to a wide range of conditions: tube diameters (equivalent diameters for non-circular channels) from 0.8 to 10 mm, mass velocities from 170 to 570 kg/m^2 s, heat fluxes from 5 to 32 kW/m^2 and saturation temperatures from −28 to 25 °C (reduced pressures from 0.21 to 0.87).

Keywords: Model; Flow boiling; Heat transfer; Flow map; Flow patterns; Flow regimes; CO_2

1. Introduction

Carbon dioxide (CO_2 or R744) has been receiving renewed interest as an efficient and environmentally safe refrigerant in a number of applications, including mobile air conditioning, heat pump systems and hot water heat pumps in recent years [1–4]. Due to its low critical temperature ($T_{crit} = 31.1$ °C) and high critical pressure ($p_{crit} = 73.8$ bar), CO_2 is utilized at much higher operating pressures compared to other conventional refrigerants. The higher operating pressures result in high vapor densities, very low surface tensions, high vapor viscosities and low liquid viscosities and thus yield flow boiling heat transfer and two-phase flow characteristics that are quite different from those of conventional refrigerants. High pressures and low surface tensions have major effects on nucleate boiling heat transfer characteristics and previous experimental studies have suggested a clear dominance of nucleate boiling heat transfer even at very high mass velocity. Therefore, CO_2 has higher heat transfer coefficients than those of conventional refrigerants at the same saturation temperature and the available heat transfer correlations generally underpredict the experimental data of CO_2. In addition, previous experimental studies have demonstrated that dryout may occur at moderate vapor quality in CO_2 flow boiling, particularly at high mass velocity and high temperature conditions. Significant deviations for the flow patterns of CO_2 compared with the flow pattern maps that

* Corresponding author. Tel.: +41 21 693 5981; fax: +41 21 693 5960.
E-mail addresses: lixincheng@hotmail.com (L. Cheng), john.thome@epfl.ch (J.R. Thome).

0017-9310/$ - see front matter © 2006 Elsevier Ltd. All rights reserved.
doi:10.1016/j.ijheatmasstransfer.2006.04.003

Nomenclature

Co	Confinement number $[\sigma/g(\rho_L - \rho_V)D^2]^{1/2}$
c_p	specific heat at constant pressure, J/kg K
D	internal tube diameter, m
D_{eq}	equivalent diameter, m
D_h	hydraulic diameter, m
D_{th}	threshold diameter, m
Fr	Froude number $[G^2/(\rho^2 gD)]$
G	total vapor and liquid two-phase mass velocity, kg/m^2 s
g	gravitational acceleration, 9.81 m/s^2
h	heat transfer coefficient, W/m^2 K
k	thermal conductivity, W/m K
M	molecular weight, kg/kmol
Pr	Prandtl number $[c_p\mu/k]$
p	pressure, Pa
p_r	reduced pressure $[p/p_{crit}]$
q	heat flux, W/m^2
Re_H	homogeneous Reynolds number $[(GD/\mu_V)[x + (1 - x)(\rho_V/\rho_L)]]$
Re_V	vapor phase Reynolds number $[GxD/(\mu_V\varepsilon)]$
S	nucleate boiling suppression factor
T	temperature, °C
We	Weber number $[G^2D/(\rho\sigma)]$
x	vapor quality
Y	correction factor

Greek symbols

δ	liquid film thickness, m
ε	cross-sectional vapor void fraction
$\bar{\varepsilon}$	average deviation, %
$\lvert\bar{\varepsilon}\rvert$	mean deviation, %
μ	dynamic viscosity, N s/m^2
θ	angle of tube perimeter, rad
ρ	density, kg/m^3
σ	surface tension, N/m; standard deviation, %

Subscripts

cb	convection boiling
crit	critical
de	dryout completion
di	dryout inception
dry	dry
dryout	dryout region
exp	experimental
IA	intermittent flow to annular flow
L	liquid
mist	mist flow
nb	nucleate boiling
pred	predicted
sat	saturation
strat	stratified flow
tp	two-phase flow
V	vapor
wavy	wavy flow
wet	on the wet perimeter

were developed for other fluids at lower pressures have been observed as well.

In order to design evaporators for these thermal systems effectively, it is very important to understand and predict the flow boiling heat transfer and two-phase flow characteristics of CO_2 inside horizontal tubes. A lot of studies on flow boiling and two-phase flow of CO_2 have been carried out in recent years to explore the fundamental aspects with respect to the characteristics of heat transfer and two-phase flow of CO_2. Thome and Ribatski [5] have recently given a review of flow boiling heat transfer and two-phase flow of CO_2 in the literature. The review addresses the extensive experimental studies on heat transfer and two-phase flow in macro-channels [6–15] and micro-channels [12,16–25], macro- and micro-scale heat transfer prediction methods for CO_2 [12–14,26] and comparisons of these methods to the experimental database. In addition, the study of CO_2 two-phase flow patterns [13,14,22,23,25] are summarized and compared to some of the leading flow pattern maps in their review. Taking into account the lack of a well-established criterion to identify macro- and micro-scale channels, Thome and Ribatski [5] arbitrary adopted a hydraulic diameter of 3 mm to segregate the databases and heat transfer models. They found that the prediction methods by [12–14] failed to predict most of macro-scale experimental data while the method proposed by Thome and El Hajal [26] for CO_2 predicted reasonably well the macro-scale database of CO_2 at low vapor qualities. They also found that small diameter data were poorly predicted by either micro-scale or macro-scale predictive methods. Based on the results for macro-scale diameters, Thome and Ribatski suggested that the method of Thome and El Hajal should be further updated to include CO_2 effects on the annular to mist flow in order to more accurately predict heat transfer coefficients at moderate/high vapor qualities. Based on this recent and comprehensive review that is recommended as a reference study, a section describing the previous studies was judged as unnecessary in this paper and the literature concerning CO_2 studies is presented in this text just when required to the development of the heat transfer model.

In the present study, the objectives are to develop a new general heat transfer prediction method and a new flow pattern map especially for CO_2, which covers channel

Table 1
The database of flow boiling heat transfer of CO_2

Data source	Channel configuration and material	D_h (mm)	T_{sat} (°C)	p_r	G (kg/m^2 s)	q (kW/m^2)	Data points	Heating method
Knudsen and Jensen [7]	Single circular tube, stainless steel	10.06	−28	0.21	80	8, 13	16	Heated by condensing R22 vapor
Yun et al. [9]	Single circular tube, stainless steel	6	5	0.54	170, 240, 340	10, 15, 20	53	Electrical heating
			10	0.61				
Yoon et al. [14]	Single circular tube, stainless steel	7.35	0	0.47	318	12.5, 16.4, 18.6	127	Electrical heating
			5	0.54				
			10	0.61				
			15	0.69				
			20	0.78				
Koyama et al. [16]	Single circular tube, stainless steel	1.8	0.3	0.47	250, 260	32.06	36	Electrical heating
			10	0.61				
			10.9	0.62				
Pettersen [20]	Multi-channel with 25 circular channels, aluminium	0.8	0	0.47	190, 280, 380, 570	5, 10, 15, 20	46	Heated by water
			10	0.61				
			20	0.78				
			25	0.87				
Yun et al. [21][a]	Multi-channels with rectangle channels	1.14 (2.7)	5	0.54	200, 300, 400	10, 15, 20	56	Electrical heating
		1.53 (3.08)						
		1.54 (3.21)						

[a] Material is not mentioned in the paper and the values in the parentheses are equivalent diameters.

diameters found in most of CO_2 flow boiling applications. Experimental conditions of studies on flow boiling of carbon dioxide covered by this study are summarized in Table 1. It includes experimental results obtained for mass velocities from 80 to 570 kg/m^2 s, heat fluxes from 5 to 32.06 kW/m^2, saturation temperatures from −28 to 25 °C (the corresponding reduced pressures are from 0.21 to 0.87) and tube diameters from 0.8 to 10.06 mm. All those experiments were conducted in horizontal tubes. Therefore, at this point, one very important issue must be clarified about the distinction between macro- and micro-channels first. Although a universal agreement to distinguish between macro- and micro-channels is not as yet clearly established, the present study covers both macro- and micro- (mini)-channels according to various criteria [27,28]. Based on engineering practice and application areas, Kandlikar [27] proposed using the following threshold diameters: conventional channels, $D_h > 3$ mm; minichannels, D_h between 200 μm and 3 mm; and micro-channels, D_h between 10 μm and 200 μm. Based on the confinement of bubble departure sizes in channels, Kew and Cornwell [28] proposed an approximate physical criterion for macro- to micro-channel threshold diameter as follows:

$$D_{th} = \left(\frac{4\sigma}{g(\rho_L - \rho_V)}\right)^{1/2} \quad (1)$$

When hydraulic diameters are larger than the threshold diameter, the channels are defined as macro-scale channels. When hydraulic diameters are smaller than the threshold diameter, the channels are defined as micro-scale channels. The test conditions of the present selected database (see Table 1) are compared to these two criteria in Fig. 1. Unlike the fixed values for the threshold diameters defined by Kandlikar, the threshold diameters based on Confinement number decrease with increasing reduced pressure and they vary from 2.3 mm at low reduced pressures to

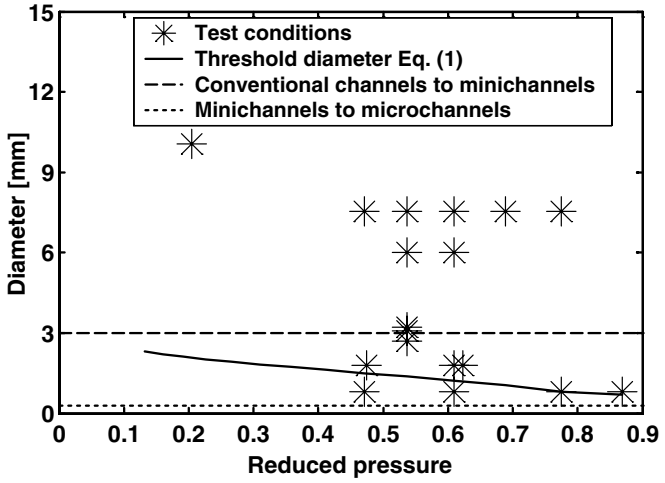

Fig. 1. Comparison of the test conditions of the database with the two criteria of threshold diameters. (Dashed lines are the criteria defined by Kandlikar [27] and solid line is the Confinement number criterion defined by Kew and Cornwell [28].)

0.7 mm at high reduced pressures. According to Kandlikar's criteria, the test conditions include both conventional and mini-channels but not micro-channels. According to the criteria based on Confinement number, *Co*, the test conditions mostly include macro-channels with a few micro-channels. Here, it is important to highlight the fact that the macro-to-micro transition should be identified by distinction in the heat transfer, pressure drop and flow patterns behaviors instead of fixed tube diameter ranges defined according to the applications. Therefore, the fact that, according to the available transition criteria, the proposed model covers both macro- and micro- (mini)-channels is perfectly reasonable since a threshold diameter based on the analysis of the heat transfer behavior of the present database was not identified.

In the present study, a new general heat transfer model and a new flow pattern map physically related to the heat transfer mechanisms based on a selected database from the literature were developed specially for CO_2. As the starting point, the model developed by Wojtan et al. [29,30] which is an updated version of the Kattan–Thome–Favrat flow pattern map and flow boiling heat transfer model [31–33] was used. The new proposed prediction method includes new correlations for the nucleate boiling heat transfer and the suppression factor based on CO_2 experimental data. In addition, a dryout inception vapor quality correlation was proposed for CO_2 and accordingly the heat transfer correlation in the dryout region was obtained. Based on the heat transfer mechanisms, a new flow patterns map was proposed and thus can physically explain the heat transfer phenomena according to the flow regimes defined by the new flow map.

2. CO_2 flow boiling heat transfer database and comparisons

2.1. Selection of CO_2 flow boiling heat transfer data

Six independent experimental studies from different laboratories have been carefully selected to form the present database for flow boiling heat transfer of CO_2. They are the experimental data of Knudsen and Jensen [7], Yun et al. [9], Yoon et al. [14], Koyama et al. [16], Pettersen [20] and Yun et al. [21]. The detailed test conditions of the database are summarized in Table 1. The test channels include single circular channels and multi-channels with circular and rectangle channels at a wide range of test conditions, by electrical heating or fluid heating. The data were taken from tables where available or by digitizing the heat transfer graphs in these publications to extract the plotted heat transfer coefficients. All together, 334 heat transfer data points including heat transfer data in the dryout region were obtained.

In order to develop a general flow boiling heat transfer prediction model, extensive comparisons of the data available in the literature have been made. However, some of the data available have not been selected due to various reasons. For example, the data of Bredesen et al. [6] for a 7 mm inside diameter tube have been excluded because they differ significantly from comparable data for 6 mm and 10.06 mm inside diameter tubes in two other studies and also because there is a large scatter among their data. Hwang et al. [34] also noted an anomaly in the [6] data at a mass velocity of 300 kg/m^2 s when correlating them. Yet, since their tests were run with the same rigor as the other tests, it is not clear where these problems come from. Also, the data of Huai et al. [17] have been excluded because the available correlations overpredict their data as indicated in their study, which contradicts the general conclusion that the available correlations underpredict experimental CO_2 data. It is unclear why they obtained the opposite trend.

In the present study, the physical properties of CO_2 have been obtained from REFPROP of NIST [35]. For non-circular channels, equivalent diameters rather than hydraulic diameters were used. Using equivalent diameter gives the same mass velocity as in the non-circular channel and thus correctly reflects the mean liquid and vapor velocities, something using hydraulic diameter does not.

2.2. Analysis of the flow boiling heat transfer data in the database

Although some anomalous data have already been excluded as pointed out earlier, the heat transfer data in the database show still some different behaviors at similar test conditions. Fig. 2(a) shows two opposite heat transfer characteristics with saturation temperature in the studies of Pettersen [20] and Yoon et al. [14]. The heat transfer coefficients increase with the increasing saturation temperatures in the study of Pettersen while they decrease in the study of Yoon et al. The only big difference between the two studies is the diameters of the test channels as indicated in Fig. 2(a). Fig. 2(b) shows the comparison of the heat transfer coefficients of Pettersen [20] to those of Koyama et al. [16]. The biggest difference between them is that in Koyama et al. the heat flux is 32.06 kW/m^2 while in Pettersen is 10 kW/m^2. The heat transfer coefficients fall off at the vapor quality of about 0.7 in the study of Pettersen while the heat transfer coefficients increase even at qualities larger than 0.7 in the study of Koyama et al. It is difficult to explain why the heat transfer coefficients fall off at the lower heat flux in one study while they still increase at the higher heat flux in the other study. This could be an effect of the heating methods or multi-channel vs. single-channel data. However, these heat transfer data of Koyama et al. at higher vapor qualities seem to be unreasonable since they should correspond to the dryout region and their trend contradicts in general with the other results. Another example of anomaly was found in the experimental data of Yun et al. [21]. According to their results, a heat transfer coefficients up to 80% higher was obtained with a very little change of hydraulic diameters from 1.53 mm to 1.54 mm at equal test conditions. Those authors have not explained why there is such a big difference even at nearly

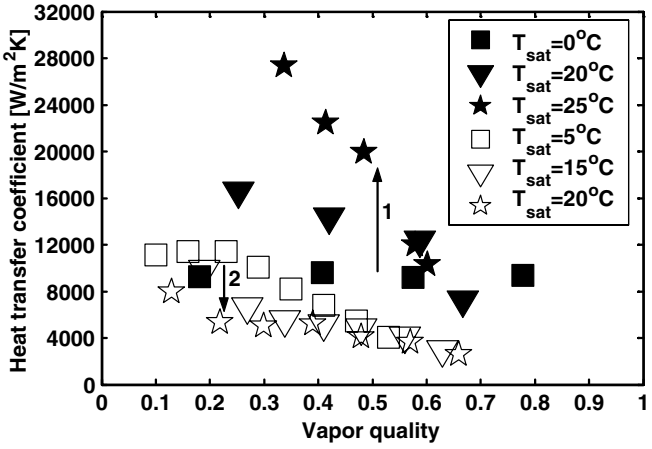

(a) The experimental flow boiling heat transfer coefficients in two different studies showing two opposite trends with the increase of saturation temperature. Arrow 1 showing the trend of the experimental flow boiling heat transfer coefficients (solid symbols) of Pettersen [20] for the conditions: $D_h = 0.8$ mm, $G = 280$ kg/m^2 s and $q = 10$ kW/m^2 at $T_{sat} = 0$, 20 and 25 °C, respectively. Arrow 2 showing the trend of the experimental flow boiling heat transfer coefficients (hollow symbols) of Yoon et al. [14] for the conditions: $D_h = 7.53$ mm, $G = 318$ kg/m^2 s and $q = 16.4$ kW/m^2 at $T_{sat} = 5$, 15 and 20 °C.

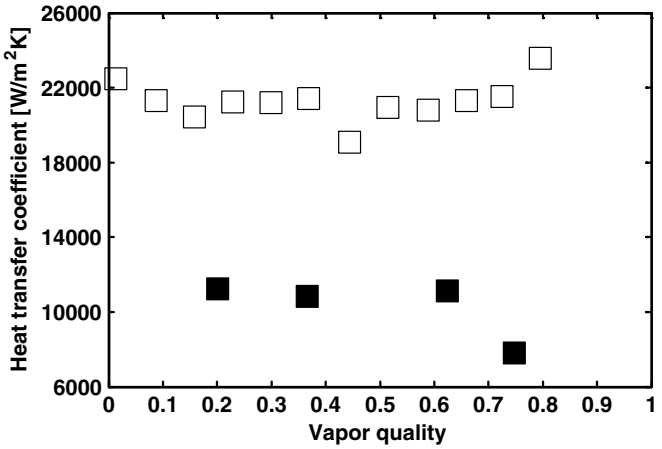

(b) The experimental flow boiling heat transfer coefficients in two different studies showing opposite flow boiling heat transfer coefficient trends. Solid symbols showing the experimental flow boiling heat transfer coefficients of Pettersen [20] for the conditions: $D_h = 0.8$ mm, $G = 190$ kg/m^2 s, $T_{sat} = 0$ °C and $q = 10$ kW/m^2 and hollow symbols showing the experimental flow boiling heat transfer coefficients of Koyama et al. [16] for the conditions: $D_h = 1.8$ mm, $G = 260$ kg/m^2 s, $T_{sat} = 0.3$ °C and $q = 32.06$ kW/m^2.

Fig. 2. Comparison of the experimental flow boiling heat transfer data in the database.

the same test conditions. In all, the experimental data from different studies show somehow different heat transfer behaviors and thus will affect the accuracy of the new heat transfer model and the new flow pattern map to be developed for CO_2 in the present study since no conclusive reasons for the contradicting trends could be found and it is not possible to say which study is right either.

3. New CO_2 flow pattern map

The new flow pattern map for CO_2 is developed according to the corresponding heat transfer mechanisms in various flow regimes. Based on the heat transfer data in the database, the intermittent flow to annular flow (I–A) and the annular flow to dryout region (A–D) transition criteria in the flow pattern map of Wojtan et al. [29] have been modified to fit the experimental data of CO_2. The new flow pattern map is intrinsically related to the corresponding heat transfer mechanisms of CO_2. To reflect the real mass flow velocities, equivalent diameters are used for non-circular channels. Other transition criteria are the same as that of Wotjan et al. Thus, based on the fact that the original publications can be easily found, the other flow patterns transition criteria by [29] will not be described here.

3.1. Modifications to the flow pattern map for CO_2

Flow patterns at diabatic conditions are intrinsically related to the corresponding flow boiling heat transfer characteristics. The flow patterns can be used to explain physically the heat transfer mechanisms and characteristics. Vice versa, the heat transfer mechanisms and characteristics can be used to backout the corresponding flow patterns. CO_2 reveals strong nucleate boiling heat transfer characteristics in intermittent flow at low vapor quality due to its physical properties. The distinction between intermittent flow and annular flow was indicated by the sharp fall-off of heat transfer coefficients between the two flow regimes. The onset of dryout inception was also observed by a sharp drop in heat transfer. Therefore, the distinction between annular flow and dryout region can be determined. Combining with the heat transfer model for CO_2 (in Section 4), the I–A and A–D transition boundaries proposed by Wotjan et al. [29] were further modified so as to fit the heat transfer characteristics. Based on the experimental data, the following I–A and A–D transition criteria are proposed for CO_2 as

1. The I–A transition boundary is calculated with the new criterion as follows:

$$x_{IA} = [1.8^{1/0.875}(\rho_V/\rho_L)^{-1/1.75}(\mu_L/\mu_V)^{-1/7} + 1]^{-1} \quad (2)$$

2. The A–D transition boundary is calculated with the new criterion as follows:

$$G_{dryout} = \left\{ \frac{1}{0.67}\left[\ln\left(\frac{0.58}{x}\right) + 0.52\right]\left(\frac{D}{\rho_V \sigma}\right)^{-0.17} \times \left[\frac{1}{gD\rho_V(\rho_L - \rho_V)}\right]^{-0.348}\left(\frac{\rho_V}{\rho_L}\right)^{-0.25}\left(\frac{q}{q_{crit}}\right)^{-0.7}\right\}^{0.965} \quad (3)$$

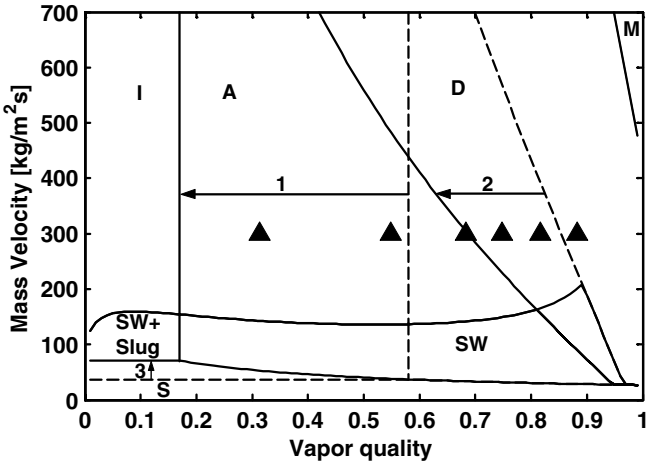

(a) The new flow pattern transition boundaries (solid lines) for CO_2 and the flow pattern transition boundaries (dashed lines) of Wojtan et al. [29] compared to the CO_2 experimental data of Yun et al. [21] (solid triangle symbols): Arrow 1 shows the change of I–A transition boundary and arrow 2 shows the change of A–D transition boundary. Arrow 3 shows the change of S–SW/SW + Slug boundary.

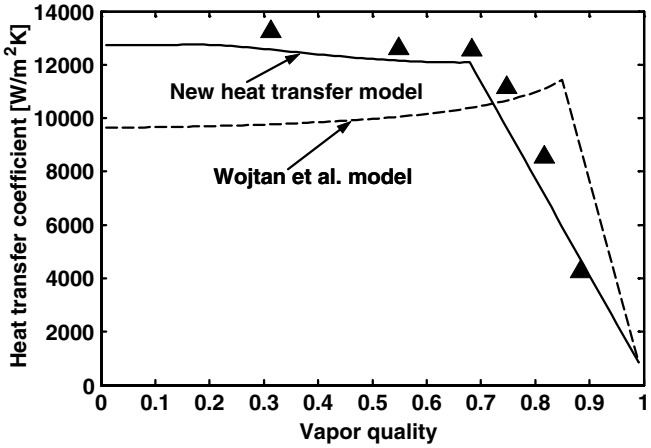

(b) Flow boiling heat transfer coefficients predicted by the new flow boiling heat transfer model for CO_2 (in Section 4) and the flow boiling heat transfer model of Wojtan et al. [30] compared with the experimental flow boiling heat transfer coefficients of Yun et al. [21].

Fig. 3. New flow pattern map for CO_2 ($D_h = 1.54$ mm, $G = 300$ kg/m^2 s, $T_{sat} = 5$ °C and $q = 20$ kW/m^2).

which is extracted from Eq. (15) (in Section 4) for the dryout inception of CO_2. In this equation, q_{crit} is calculated according to Kutateladze [36]. For non-circular channels, equivalent diameters are used.

3.2. Comparison of the new flow pattern map for CO_2 to experimental data

Fig. 3(a) shows the comparison of the new flow pattern map for CO_2 and the flow pattern map of Wojtan et al. to the experimental data of Yun et al. [21] at the indicated test conditions (in the flow pattern map, A stands for annular flow, D stands for dryout region, I stands for intermittent flow, M stands for mist flow, S stands for stratified flow and SW stands for stratified-wavy flow. The stratified to stratified-wavy flow transition is designated as S–SW, the stratified-wavy to intermittent/annular flow transition is designated as SW–I/A, the intermittent to annular flow transition is designated as I–A and so on.). Arrow 1 shows the change of I–A transition boundaries and arrow 2 shows the change of A–D transition boundaries from the flow pattern map of Wojtan et al. to the new flow pattern map for CO_2. Arrow 3 shows the changes of the S–SW/Slug + SW transition boundaries that are automatically changed due to the change of I–A and A–D transition boundaries. Other transition boundaries are the same. Fig. 3(b) shows the corresponding comparison of the predicted heat transfer coefficients with the heat transfer model of Wojtan et al. and the new heat transfer model for CO_2 (in Section 4) to the experimental data at the same conditions as that in Fig. 3(a). Obviously, the flow pattern map of Wojtan et al. cannot reflect the corresponding CO_2 heat transfer characteristics correctly and the heat transfer model of Wojtan et al. predicts poorly the experimental heat transfer coefficients of CO_2. The new CO_2 flow pattern map reflects the heat transfer mechanisms well in the corresponding flow regimes and the CO_2 heat transfer model predicts the corresponding CO_2 experimental heat transfer coefficients well. The heat transfer coefficients start to fall in the A–D transition due to the inception of dryout at the top of the tube and then fall off sharply in the dryout region. The predicted and the experimental heat transfer coefficients are in good agreement in these flow regimes. It should be mentioned here that there are only two studies of flow visualization of CO_2 flow boiling [23,24] in the literature. Unfortunately, neither contains the corresponding study of heat transfer characteristics which should be related to the observed flow patterns. In addition, in the study of Yun et al. [23], the maximum mass velocity reaches 1500 kg/m^2 s, which is much higher than the maximum value 570 kg/m^2 s in the present database and their heat flux is 100 kW/m^2, which is also much higher than the maximum heat flux 32 kW/m^2 in the present database. In the study of Pettersen [24], it is difficult to interpret some of his observations by his definitions of the flow regimes in our flow pattern map. It is also difficult to judge some of his flow regimes so as to compare to the new flow pattern map.

4. New flow boiling heat transfer model for CO_2

It is a formidable task to develop a general flow boiling heat transfer model for CO_2 because of the diversities of the heat transfer trends in the database. To develop a general prediction method, it is important that the method is

not only numerically accurate but that it captures correctly the trends in the data. Most importantly, the heat transfer mechanisms should be related to the corresponding flow patterns and be physically explained according to flow pattern transitions. Accordingly, a new general heat transfer model is proposed here using the Wojtan et al. [30] model as our starting point. Equivalent diameters are used for non-circular channels.

4.1. Brief description of the flow boiling heat transfer model of Wojtan et al.

Wojtan et al. [30] extended the Kattan–Thome–Favrat [31–33] heat transfer model to include dryout region and mist flow heat transfer methods and improved the heat transfer prediction in stratified-wavy flows. The Kattan–Thome–Favrat general equation for the local heat transfer coefficients h_{tp} in a horizontal tube is

$$h_{tp} = \left[\theta_{dry} h_V + (2\pi - \theta_{dry}) h_{wet}\right]/2\pi \quad (4)$$

where θ_{dry} is the dry angle as shown in Fig. 4. The dry angle defines the flow structures and the ratio of the tube perimeters in contact with liquid and vapor. In stratified flow, θ_{dry} equals the stratified angle, θ_{strat}, which is calculated according to Thome and El Hajal [37]. In annular and intermittent flows, $\theta_{dry} = 0$. For stratified-wavy flow, θ_{dry} varies from zero up to its maximum value θ_{strat}. Wojtan et al. subdivided the stratified-wavy flow into three subzones (slug, slug/stratified-wavy and stratified-wavy). Based on the fact that the high frequency slugs maintain a continuous thin liquid layer on the upper tube perimeter, θ_{dry} is defined equal to 0 in the slug zone. The dry angles in the slug/stratified-wavy and stratified-wavy regions are calculated according to equations developed by Wojtan et al. [30] based in exponential interpolations giving smooth transition in the determination of dry angle between respective zones and also a smooth transition in the heat transfer coefficient from zone to zone.

The vapor phase heat transfer coefficient on the dry perimeter h_V is calculated with the Dittus–Boelter [38] correlation assuming tubular flow in the tube:

$$h_V = 0.023 Re_V^{0.8} Pr_V^{0.4} (k_V/D) \quad (5)$$

and the heat transfer coefficient on the wet perimeter is calculated with an asymptotic model that combines the nucleate boiling and convective boiling contributions to the heat transfer by the third power:

$$h_{wet} = \left[(h_{nb})^3 + h_{cb}^3\right]^{1/3} \quad (6)$$

In this equation, the correlation proposed by Cooper [39] multiplied by a fixed boiling suppression factor of 0.8 is used to calculate the nucleate boiling contribution. The convective contribution is calculated with the following correlation assuming a liquid film flow:

$$h_{cb} = 0.0133 \left(\frac{4G(1-x)\delta}{\mu_L(1-\varepsilon)}\right)^{0.69} Pr_L^{0.4} \frac{k_L}{\delta} \quad (7)$$

where the term in the bracket is the liquid film Reynolds number. In this equation, the void fraction is determined with the Rouhani and Axelsson [40] drift flux model (as in [29–33]) and the liquid film thickness is calculated as suggested by El Hajal et al. [41].

The heat transfer coefficient in mist flow is calculated as follows [30]:

$$h_{mist} = 0.0117 Re_H^{0.79} Pr_V^{1.06} Y^{-1.83} (k_V/D) \quad (8)$$

where Re_H is the homogeneous Reynolds number and Y is the correction factor originally proposed by Groeneveld [42] and given by

$$Y = 1 - 0.1\left[(\rho_L/\rho_V - 1)(1-x)\right]^{0.4} \quad (9)$$

The heat transfer coefficient in the dryout region is calculated by proration as [30]

$$h_{dryout} = h_{tp}(x_{di}) - \frac{x - x_{di}}{x_{de} - x_{di}} \left[h_{tp}(x_{di}) - h_{mist}(x_{de})\right] \quad (10)$$

where $h_{tp}(x_{di})$ is the two-phase flow heat transfer coefficient calculated from Eq. (4) at the dryout inception quality x_{di} and $h_{mist}(x_{de})$ is the mist flow heat transfer coefficient calculated from Eq. (8) at the dryout completion quality x_{de}. If x_{de} is not defined at the considered mass velocity it is assumed that $x_{de} = 0.999$. For more details about the flow boiling heat transfer model and flow patterns map proposed by Wotjan et al. [29,30], we suggest to consult the original papers.

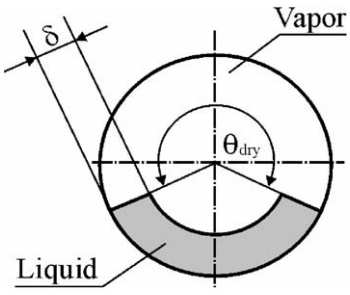

Fig. 4. Schematic diagram of annular flow with partial dryout.

4.2. Modifications in the new flow boiling heat transfer model for CO_2

Like any other flow boiling heat transfer model, both the Kattan–Thome–Favrat model and the modified model of Wojtan et al. drastically underpredicts the heat transfer coefficients for CO_2, particularly at low and intermediate vapor qualities as shown in Fig. 3(b). Moreover, CO_2 at high saturation pressures gives a trend of a monotonic decrease in heat transfer coefficient versus vapor quality in intermittent and annular flows, which is the exact opposite of the trend for other refrigerants such as R-134a at low pressures [8,9]. The nucleate boiling contribution is much larger than the convective boiling contribution for CO_2 while the opposite is true for R-134a. Hence,

suppression of nucleate boiling acts on the heat transfer coefficients of CO_2 to greatly reduce its contribution to the heat transfer with the increase of vapor quality. Therefore, to develop a general model for CO_2, first, a new nucleate boiling heat transfer correlation is needed especially for CO_2. Then, a reasonable suppression factor is needed so as to capture the correct parametric trend of CO_2. Furthermore, a correlation of dryout inception is needed so as to predict accurately the heat transfer in dryout region by considering the fact that the dryout phenomenon of CO_2 occurs much earlier than that of other refrigerants. All these aspects should be based on physically reasonable grounds as the heat transfer mechanisms are intrinsically related to the corresponding flow patterns.

4.2.1. Development of a new nucleate boiling heat transfer correlation for CO_2

The experimental heat transfer data at vapor qualities $x < x_{IA}$ in the CO_2 database were evaluated to extract the nucleate boiling contribution to develop a new nucleate boiling heat transfer correlation for CO_2. The data were first set equal to h_{tp} in Eq. (4) and then the vapor phase and the convective boiling heat transfer contributions were removed utilizing Eqs. (5) and (7), yielding the nucleate boiling heat transfer contribution from Eq. (6). Thome and EI Hajal [26] used the experimental data at vapor qualities $x < 0.2$ to extract h_{nb} data from their database and proposed a modified nucleate boiling heat transfer correlation, which is a simple linear correction to the Cooper [39] correlation. From the viewpoint of physical mechanisms, it is more reasonable to use the intermittent flow to annular flow transition vapor quality than to use a fixed vapor quality 0.2 as the distinct line to extract the nucleate boiling heat transfer data. Moreover, their form of the modified nucleate boiling correlation cannot explain physically the nucleate boiling heat transfer of CO_2 although it could predict the data correctly. By comparing the experimental h_{nb} with the predicted values by the modified nucleate boiling correlation of Thome and El Hajal [26], the Cooper [39] correlation and the fluid-specific correlation of Gorenflo [43], it has been found that the correlation of Thome and El Hajal predicts well the experimental data at low heat flux while it overpredicts them at high heat flux with errors exceeding 40% for some cases, perhaps because their linear form of correction does not reflect the actual variation of nucleate boiling heat transfer at higher heat fluxes. The Cooper correlation underpredicts the experimental nucleate boiling heat transfer data at low heat fluxes. The correlation of Gorenflo overpredicts the experimental nucleate boiling heat transfer data by a large margin with the errors are mostly from 40% to 60%. The reason could be the lack of extensive data of CO_2 in setting their standardized value for CO_2. Thus, it is necessary to develop a new nucleate boiling heat transfer correlation for CO_2.

In order to develop the new nucleate boiling correlation for CO_2, reduced pressure is one key factor verified by the previous experimental studies. So the reduced pressure based Cooper correlation is used to modify the nucleate boiling heat transfer for CO_2. By analyzing and comparing the nucleate boiling heat transfer data, it was found that the heat flux term in the Cooper correlation did not reflect the real trend for CO_2 nucleate boiling heat transfer. Thus, the exponent of the heat flux was newly determined based on the nucleate boiling data of CO_2, and a value of 0.58 compared to the original value of 0.67. Then, the reduced pressure term was correlated based on the nucleate boiling heat transfer data of CO_2 by keeping the logarithmic and molecular terms in the Cooper correlation unchanged. The following new nucleate boiling heat transfer correlation was obtained:

$$h_{nb} = 131 p_r^{-0.0063} (-\log_{10} p_r)^{-0.55} M^{-0.5} q^{0.58} \quad (11)$$

Fig. 5 shows the comparison of the predicted nucleate boiling heat transfer coefficients by the new nucleate boiling heat transfer correlation for CO_2 with the present database. About 90% of the experimental nucleate boiling heat transfer coefficients are predicted within ±20%.

4.2.2. Development of a nucleate boiling heat transfer suppression factor correlation for CO_2

As nucleate boiling heat transfer is suppressed in annular flow, a boiling suppression factor correlation is needed in the flow boiling heat transfer model for CO_2 so as to capture the trend of heat transfer characteristics. To develop the boiling suppression factor correlation for CO_2, first the physical mechanisms of flow boiling heat transfer are considered and secondly the effect of tube diameters. Unlike other boiling suppression factor correlations such as in Chen [44] and Gungor and Winterton [45] correlations, which were empirically correlated based on the Lockhart–Martinelli number, Reynolds number, Boiling number, Prandtl number and so on, liquid film thickness is used as a main parameter in the present study. The Cooper correlation was first replaced with the new nucleate boiling heat transfer correlation. Then, the boiling

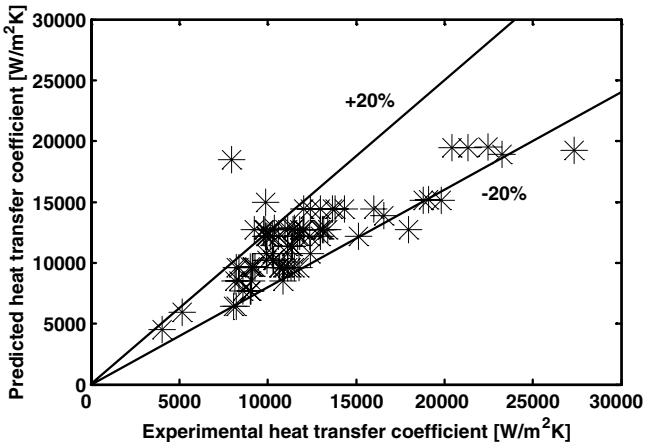

Fig. 5. Comparison of the predicted nucleate boiling heat transfer coefficients by the nucleate boiling heat transfer correlation for CO_2 with the experimental nucleate boiling heat transfer coefficients.

suppression factors were backed out of the whole database (except the dryout data points). Incorporating the effect of tube diameter, the following boiling suppression factor correlation was obtained for CO_2:

$$\text{If } x < x_{IA}, \quad S = 1 \tag{12}$$

$$\text{If } x \geqslant x_{IA}, \quad S = 1 - 1.14(D/D_{ref})^2(1 - \delta/\delta_{IA})^{2.2} \tag{13}$$

where $D_{ref} = 0.00753$ m.

Furthermore, if $D > 7.53$ mm, then set $D = 7.53$ mm. For non-circular channels, the equivalent diameter is used. The correlation is applicable to the conditions: $-28\ ^\circ\text{C} \leqslant T_{sat} \leqslant 25\ ^\circ\text{C}$, $5\ \text{kW/m}^2 \leqslant q \leqslant 32\ \text{kW/m}^2$, $170\ \text{kg/m}^2\,\text{s} \leqslant G \leqslant 570\ \text{kg/m}^2\,\text{s}$, $0.8\ \text{mm} \leqslant D \leqslant 10\ \text{mm}$.

Combining the nucleate boiling heat transfer correlation for CO_2 and the nucleate boiling heat transfer suppression factor correlation, the flow boiling heat transfer coefficients on the wet perimeter are calculated according to the following:

$$h_{wet} = [(S \cdot h_{nb})^3 + h_{cb}^3]^{1/3} \tag{14}$$

4.2.3. New dryout region heat transfer correlation for CO_2

Some of the flow boiling heat transfer data of CO_2 in the database contain obviously the dryout points as the heat transfer coefficients fall off sharply. In the process of developing the boiling suppression factor correlation, the dryout data were determined according to the corresponding boiling suppression factors. Those giving negative boiling suppression factor values were taken as the dryout points and the data giving boiling suppression factor values around zero were taken as indicating the onset of the dryout. Based on the dryout inception data, the dryout inception vapor quality correlation of Wojtan et al. was modified and thus a new annular to dryout region (A–D) transition boundary in the flow pattern map was extracted from the modified dryout inception vapor quality correlation Eq. (15) for CO_2. By comparing the new flow pattern map with the experimental data, the dryout inception vapor quality correlation was further modified according to the heat transfer characteristics and mechanisms together with the corresponding flow regimes. The new dryout inception vapor quality correlation is

$$x_{di} = 0.58\exp\left(\left[0.52 - 0.67We_V^{0.17}Fr_V^{0.348}(\rho_V/\rho_L)^{0.25}(q/q_{crit})^{0.7}\right]\right) \tag{15}$$

Based on the new dryout inception vapor quality correlation, the new A–D transition criterion (Eq. (3)) for CO_2 was obtained as pointed out in Section 3.1. The dryout inception vapor qualities are calculated with Eq. (15) and thus the heat transfer coefficients in the dryout region are calculated with Eq. (10). The dryout completion vapor quality is $x_{de} = 0.999$ as suggested by Wojtan et al. [30] due to the lack of the experimental data for CO_2.

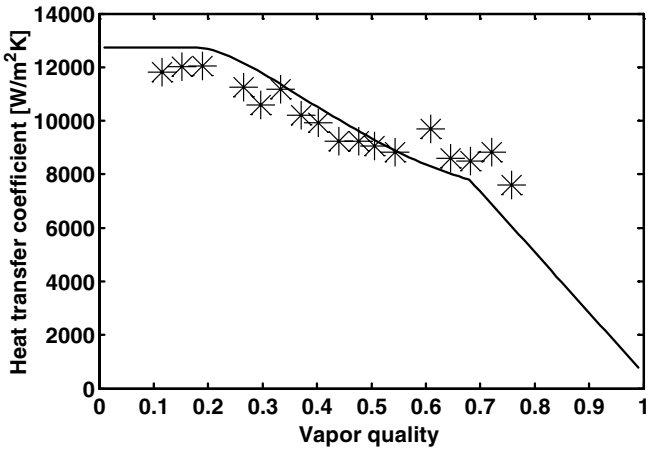

Fig. 7. Comparison of the predicted flow boiling heat transfer coefficients with the experimental flow boiling heat transfer coefficients of Yun and Kim [9] ($D_h = 6$ mm, $T_{sat} = 5\ ^\circ$C, $G = 340\ \text{kg/m}^2\,\text{s}$, $q = 20\ \text{kW/m}^2$).

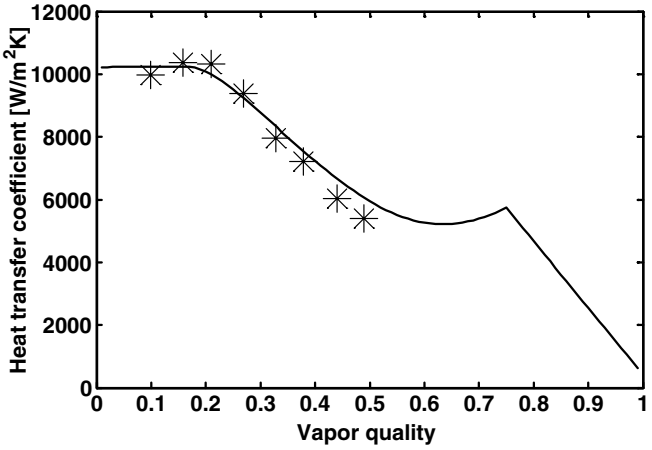

Fig. 6. Comparison of the predicted flow boiling heat transfer coefficients with the experimental flow boiling heat transfer coefficients of Yoon et al. [14] ($D_h = 7.35$ mm, $T_{sat} = 0\ ^\circ$C, $G = 318\ \text{kg/m}^2\,\text{s}$, $q = 16.4\ \text{kW/m}^2$).

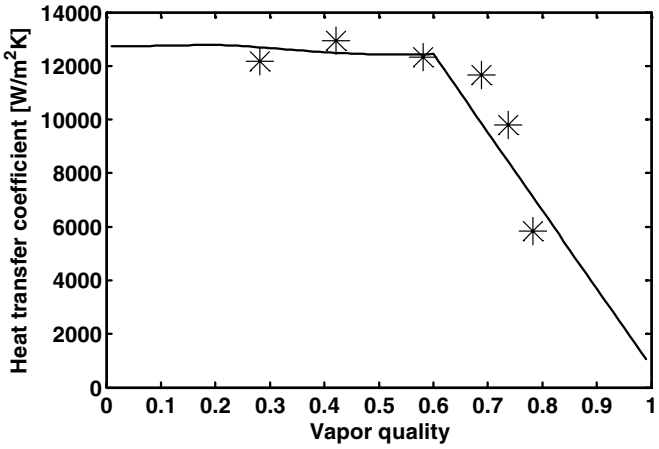

Fig. 8. Comparison of the predicted flow boiling heat transfer coefficients with the experimental flow boiling heat transfer coefficients of Yun et al. [21] ($D_h = 1.14$ mm, $T_{sat} = 5\ ^\circ$C, $G = 400\ \text{kg/m}^2\,\text{s}$, $q = 20\ \text{kW/m}^2$).

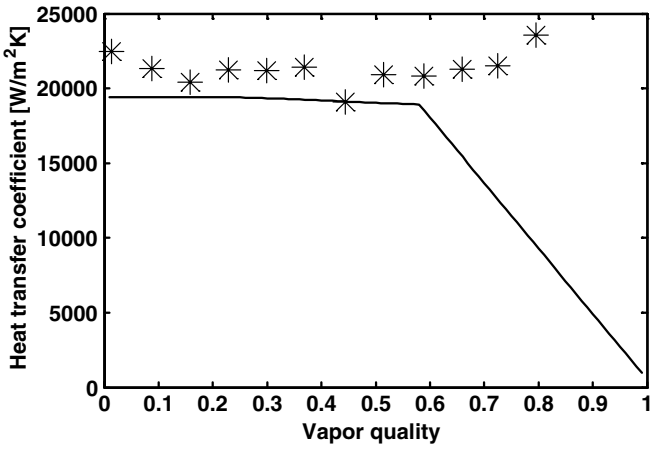

Fig. 9. Comparison of the predicted flow boiling heat transfer coefficients with the experimental flow boiling heat transfer coefficients of Koyama et al. [16] ($D_h = 1.8$ mm, $T_{sat} = 10.9$ °C, $G = 260$ kg/m^2 s, $q = 32.06$ kW/m^2).

4.3. Comparisons of the new flow boiling heat transfer model to the database

As indicated in the forgoing, the general flow boiling heat transfer model is proposed for CO_2 which incorporates the new nucleate boiling heat transfer correlation, the new boiling suppression factor correlation and the new modified dryout region heat transfer correlation. In order to verify the new flow boiling heat transfer model, the whole experimental database were used to evaluate the new heat transfer model. Figs. 6–10 show the comparisons of the predicted with the experimental heat transfer coefficients at the indicated test conditions. Generally, the new heat transfer model predicts the experimental heat transfer coefficients and captures the trends of the experimental heat transfer coefficients except for those of Koyama et al. at high vapor qualities, as shown in Fig. 9, and the entire data of Knudesen and Jensen et al. as shown in Fig. 10(b). As already shown in Fig. 2(b), the experimental data of Koyama et al. reveal an opposite trend compared to most of the other data. According to the new flow pattern map for CO_2, these data at high vapor quality should be in the dryout region and the heat transfer coefficients should show a decrease with the increasing vapor quality while instead they show an increase. The new heat transfer model poorly predicts the data of Knudsen as shown in Fig. 10(b). Apparently, the flow pattern of their data is in the stratified wavy flow region as shown in the corresponding flow pattern map in Fig. 10(a). This is confirmed by the measured temperatures in the top, middle and bottom positions as shown in their paper. The temperatures at the top are higher than that at the bottom, which means that the top of the tube was in contact with vapor and the bottom of the tube was in contact with liquid. In order to find the reason why the predicted heat transfer coefficients are much lower than the experimental data, the new flow heat transfer model was artificially changed to predict the heat transfer coefficients in the annular flow region for the same test conditions as shown by the dashed line in Fig. 10(b). The predicted heat transfer coefficients are still lower than the experimental heat transfer coefficients even assuming the flow is annular. Fortunately, some of the data of Yun and Kim [9] at a mass velocity of 170 kg/m^2 s are in or near the stratified-wavy region as shown in Fig. 11(a) and thus can be used to evaluate the new heat transfer model in the stratified-wavy flow region

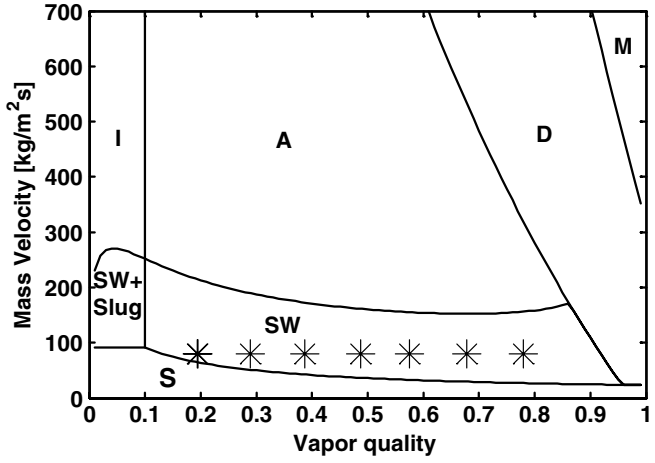

(a) Comparison of the flow pattern map to the experimental data.

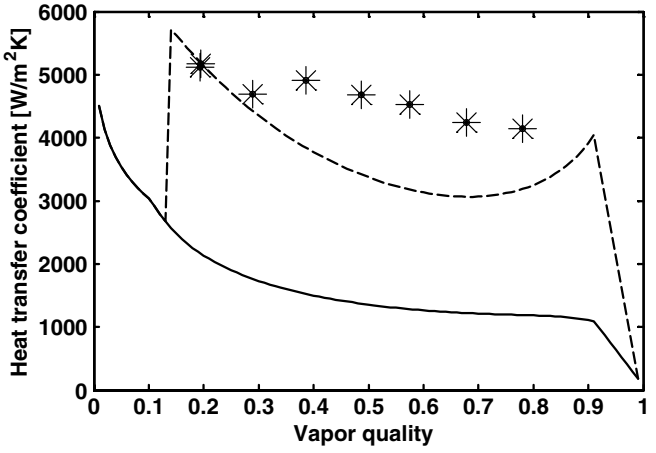

(b) Comparison of the predicted flow boiling heat transfer coefficients (solid line) with the experimental flow boiling heat transfer coefficients. (Dashed line is the predicted flow boiling heat transfer coefficients by the flow boiling heat transfer model for CO_2 assuming that the flow pattern is in annular flow region.)

Fig. 10. Comparison of the flow boiling heat transfer model for CO_2 and the corresponding flow pattern map to the experimental flow boiling heat transfer data of Knudsen and Jensen [7] ($D_h = 10.06$ mm, $T_{sat} = -28$ °C, $G = 80$ kg/m^2 s, $q = 8$ kW/m^2).

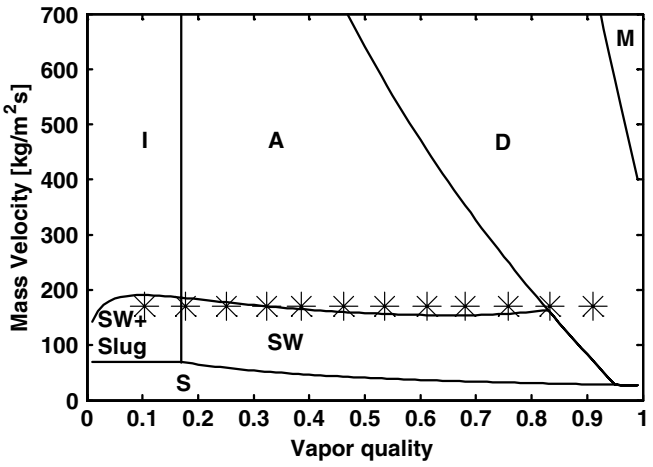

(a) Comparison of the flow pattern map to the experimental data.

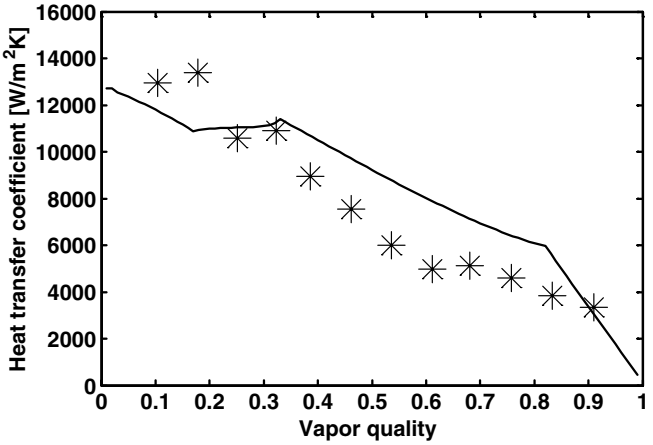

(b) Comparison of the predicted flow boiling heat transfer coefficients with the experimental flow boiling heat transfer coefficients.

Fig. 11. Comparison of the flow boiling heat transfer model for CO_2 and the corresponding flow pattern map to the experimental flow boiling heat transfer data of Yun et al. [9] ($D_h = 6$ mm, $T_{sat} = 5$ °C, $G = 170$ kg/m^2 s, $q = 20$ kW/m^2).

as well. Fig. 11(b) shows the comparison of the predicted heat transfer coefficients with the experimental data of Yun and Kim [9] at the indicated test conditions. The experimental heat transfer coefficients of Yun and Kim in the stratified-wavy flow region are well predicted by the new model. To further find the reason why the new heat transfer model under predict the experimental heat transfer coefficients of Knudesen and Jensen et al., the experimental and data reduction methods in their study have been analyzed. The test section is a stainless tube with a length of 1.12 m, an inside diameter of 10.06 mm and an outside diameter of 30 mm. The test tube was heated by condensing R22 vapor on the outside of the tube. However, how the total heat transferred to the test section was determined is not mentioned in their paper. The total heat transferred to the test section could be a key factor that caused the big discrepancy here. In addition, heating by condensation gives a constant temperature boundary rather than a uniform heat flux boundary. So, it seems that using the average temperature of the 12 measured temperatures at three different positions together with the total heat flux to calculate the inside wall temperature may be unreasonable. Therefore, their data are excluded in the following statistical analysis.

Fig. 12 shows the comparison of the predicted and experimental heat transfer coefficients for the whole experimental database. The statistical analysis of the predicted results are listed in Table 2. 75.5% of the whole experimental database are predicted within ±30% and 79.1% of the experimental data without dryout points are predicted ±30%. As for such a wide range of experimental data from different laboratories, especially some of the experimental data showing opposite heat transfer behaviors, the predicted results are quite reasonable and encouraging. Due to the lack of the dryout completion data, the prediction for the dryout region heat transfer is worse than that for the other flow regimes. It could be improved in the future if some of the experimental dryout completion data become available.

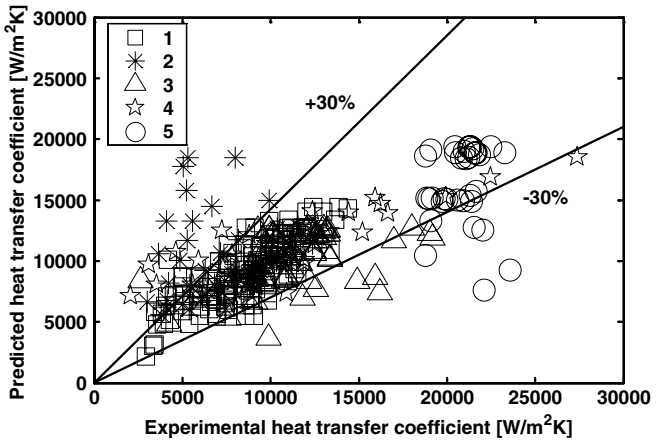

Fig. 12. Comparison of the predicted flow boiling heat transfer coefficients with the entire experimental flow boiling heat transfer database (1 – [9], 2 – [14], 3 – [21], 4 – [20] and 5 – [16]).

Table 2
Statistical analysis of the predicted results

Data used for comparison	Data points	Percentage of predicted points within ±30%	Mean deviation, $\|\bar{\varepsilon}\|$ (%)	Standard deviation, σ (%)
All data points	318	75.5	27.1	47.2
Data without dryout points	287	79.1	23.5	47.5

5. Conclusions

A new flow boiling heat transfer model and a new flow pattern map for two-phase flow in horizontal tubes have

been developed specifically for CO_2. The new flow pattern map and the new heat transfer model are intrinsically related each other. Compared to the CO_2 heat transfer model of Thome and El Hajal, several key aspects have been improved. First, a nucleate boiling heat transfer correlation is proposed for CO_2 according to the effect of heat flux and reduced pressure on nucleate boiling heat transfer at low vapor qualities. Secondly, a nucleate boiling suppression factor correlation is proposed based on the liquid film thickness and the effect of tube diameter on heat transfer. In addition, a dryout inception vapor quality correlation is proposed for CO_2 and accordingly the heat transfer correlation in the dryout region is obtained. Based on the heat transfer mechanisms, a new flow patterns map is proposed and thus can physically explain the heat transfer phenomena according to the flow regimes defined by the new flow map. The new heat transfer model predicts 75.5% of the CO_2 database (318 data points) to within $\pm 30\%$ and 79.1% of the CO_2 database (287) without dryout data points. The heat transfer model and the corresponding flow pattern map are applicable to a wide range of conditions: tube diameters (equivalent diameter for non-circular channels) from 0.8 to 10 mm, mass velocities from 85 to 570 kg/m^2 s, heat fluxes from 5 to 32 kW/m^2 and saturation temperatures from -25 to $+25$ °C.

Acknowledgements

Dr. Lixin Cheng is an Alexander von Humboldt Research Fellow in the Institute of Process Engineering at the University of Hannover in Germany and was a visiting Research Fellow in the Laboratory of Heat and Mass Transfer at Swiss Federal Institute of Technology (Lausanne) in Switzerland from January to March 2005. The visit was sponsored by a European Research Fellowship of the Alexander von Humboldt Foundation and the research is supported by the Alexander von Humboldt Foundation. Dr. Leszek Wojtan is supported by the Swiss FN contract number 510.597.

References

[1] L. Lorentzen, Revival of carbon dioxide as refrigerant, Int. J. Refrigeration 17 (1994) 292–301.
[2] P. Neksa, H. Reksta, G.R. Zakeri, P.A. Schiefloe, CO_2 heat pump water heater characteristics, system design and experimental results, Int. J. Refrigeration 21 (1998) 172–179.
[3] K. Klöcker, E.L. Schmidt, F. Steimle, Carbon dioxide as a working fluid in drying heat pumps, Int. J. Refrigeration 24 (2001) 100–107.
[4] P. Neksa, CO_2 heat pump systems, Int. J. Refrigeration 25 (2002) 421–427.
[5] J.R. Thome, G. Ribatski, State-of-the art of flow boiling and two-phase flow of CO_2 in macro- and micro-channels, Int. J. Refrigeration 28 (2006) 1149–1168.
[6] A. Bredesen, A. Hafner, J. Pettersen, P. Neksa, K. Aflekt, Heat transfer and pressure drop for in-tube evaporation of CO_2, in: Proceedings of the International Conference in Heat Transfer Issues in Natural Refrigerants, University of Maryland, USA, 1997, pp. 1–15.
[7] H.J. Knudsen, R.H. Jensen, Heat transfer coefficient for boiling carbon dioxide, in: Workshop Proceedings – CO_2 Technologies in Refrigeration, Heat Pumps and Air Conditioning Systems, Trondheim, Norway, 1997, pp. 319–328.
[8] R. Yun, J.H. Hwang, Y.C. Kim, M.S. Kim, Evaporation heat transfer characteristics of carbon dioxide in a horizontal smooth tube, IIR Commission B1 Meeting, Paderborn, Germany, 2001, pp. 519–525.
[9] R. Yun, Y. Kim, M.S. Kim, Y. Choi, Boiling heat transfer and dryout phenomenon of CO_2 in a horizontal smooth tube, Int. J. Heat Mass Transfer 46 (2003) 2353–2361.
[10] S. Jeong, D. Jeong, J.J. Lee, Evaporating heat transfer and pressure drop inside helical coils with the refrigerant carbon dioxide, in: 21st IIR International Congress of Refrigeration, Washington DC, USA, 2003, paper ICR0260.
[11] N.N. Sawant, M.S. Kim, W. Vance Payne, P.A. Domanski, Y.W. Hwang, A study of in-tube evaporation heat transfer of carbon dioxide, in: 21st IIR International Congress of Refrigeration, Washington DC, USA, 2003, paper ICR0038.
[12] J. Wang, S. Ogasawara, E. Hihara, Boiling heat transfer and air coil evaporator of carbon dioxide, in: 21st IIR International Congress of Refrigeration, Washington DC, USA, 2003, paper ICR0231.
[13] S.H. Yoon, E.S. Cho, M.S. Kim, Y. Kim, Studies on the evaporative heat transfer and pressure drop of carbon dioxide near the critical point, in: 21st IIR International Congress of Refrigeration, Washington DC, USA, 2003, paper ICR0477.
[14] S.H. Yoon, E.S. Cho, Y.W. Hwang, M.S. Kim, K. Min, Y. Kim, Characteristics of evaporative heat transfer and pressure drop of carbon dioxide and correlation development, Int. J. Refrigeration 27 (2004) 111–119.
[15] S. Koyama, S. Lee, D. Ito, K. Kuwahara, H. Ogawa, Experimental study on flow boiling of pure CO_2 and CO_2–oil mixtures inside horizontal smooth and micro-fin copper tubes, in: Proceedings of 6th IIR-Gustav Lorentzen Conference, Glasgow, UK, 2004, paper 1/A/1.40.
[16] S. Koyama, K. Kuwahara, E. Shinmura, S. Ikeda, Experimental study on flow boiling of carbon dioxide in a horizontal small diameter tube, in: IIR Commission B1 Meeting, Paderborn, Germany, 2001, pp. 526–533.
[17] X. Huai, S. Koyama, T.S. Zhao, E. Shinmura, K. Hidehiko, M. Masaki, An experimental study of flow boiling characteristics of carbon dioxide in multiport mini channels, Appl. Thermal Eng. 24 (2004) 1443–1463.
[18] H. Ohta, Boiling two-phase flow in channels with extremely small dimensions – review of Japanese research, in: 2nd International Conference on Microchannels and Minichannels, Rochester, USA, 2004, pp. 97–108.
[19] V. Siegismund, M. Kauffeld, Influence of lubricant oil on CO_2 heat transfer in minichannel tubes, in: Proceedings of 6th IIR-Gustav Lorentzen Conference, Glasgow, UK, 2004, paper 1/B/2.20.
[20] J. Pettersen, Flow vaporization of CO_2 in microchannel tubes, Exp. Thermal Fluid Sci. 28 (2004) 111–121.
[21] R. Yun, Y. Kim, M.S. Kim, Convective boiling heat transfer characteristics of CO_2 in microchannels, Int. J. Heat Mass Transfer 48 (2005) 235–242.
[22] R. Yun, Y. Kim, M.S. Kim, Two-phase flow patterns of CO_2 in a narrow rectangular channel, in: 21st IIR International Congress of Refrigeration, Washington DC, USA, 2003, paper ICR0155.
[23] R. Yun, Y. Kim, Flow regimes for horizontal two-phase flow of CO_2 in a heated narrow rectangular channel, Int. J. Multiphase Flow 30 (2004) 1259–1270.
[24] J. Pettersen, Two-phase flow patterns in microchannel vaporization of CO_2 at near-critical pressure, Heat Transfer Eng. 25 (2004) 52–60.
[25] R. Yun, Y. Kim, Critical quality prediction for saturated flow boiling of CO_2 in horizontal small diameter tubes, Int. J. Heat Mass Transfer 46 (2003) 2527–2535.
[26] J.R. Thome, J. El Hajal, Flow boiling heat transfer to carbon dioxide: general prediction method, Int. J. Refrigeration 27 (2004) 294–301.

[27] S.G. Kandlikar, Fundamental issues related to flow boiling in minichannels and microchannels, Exp. Thermal Fluid Sci. 26 (2002) 38–47.
[28] P.A. Kew, K. Cornwell, Correlations for the prediction of boiling heat transfer in small-diameter channels, Appl. Thermal Eng. 17 (1997) 705–715.
[29] L. Wojtan, T. Ursenbacher, J.R. Thome, Investigation of flow boiling in horizontal tubes: part I – a new diabatic two-phase flow pattern map, Int. J. Heat Mass Transfer (2005) 2955–2969.
[30] L. Wojtan, T. Ursenbacker, J.R. Thome, Investigation of flow boiling in horizontal tubes: part II – development of a new heat transfer model for stratified-wavy, dryout and mist flow regimes, Int. J. Heat Mass Transfer (2005) 2970–2985.
[31] N. Kattan, J.R. Thome, D. Favrat, Flow boiling in horizontal tubes. Part 1: Development of a diabatic two-phase flow pattern map, J. Heat Transfer 120 (1998) 140–147.
[32] N. Kattan, J.R. Thome, D. Favrat, Flow boiling in horizontal tubes: part 2 – new heat transfer data for five refrigerants, J. Heat Transfer 120 (1998) 148–155.
[33] N. Kattan, J.R. Thome, D. Favrat, Flow boiling in horizontal tubes: part – 3: development of a new heat transfer model based on flow patterns, J. Heat Transfer 120 (1998) 156–165.
[34] Y. Hwang, B.H. Kim, R. Radermacher, Boiling heat transfer correlation for carbon dioxide, in: Proceedings of International Conference on Heat Transfer Issues in Natural Refrigerants, November, University of Maryland, USA, 1997, pp. 81–94.
[35] REFPROP. NIST Refrigerant Properties Database 23, Gaithersburg, MD, 1998, version 6.01.
[36] S.S. Kutateladze, On the transition to film boiling under natural convection, Kotloturbostroenie (3) (1948) 10–12.
[37] J.R. Thome, J. El Hajal, Two-phase flow pattern map for evaporation in horizontal tubes: Latest version, in: 1st International Conference on Heat Transfer, Fluid Mechanics and Thermodynamics, Kruger Park, South Africa, vol. 1, April 8–10, 2002, pp. 182–188.
[38] F.W. Dittus, L.M.K. Boelter, Heat transfer in automobile radiator of the tubular type, Univ. Calif. Publ. Eng. 2 (13) (1930) 443–461.
[39] M.G. Cooper, Heat flow rates in saturated nucleate pool boiling – a wide-ranging examination of reduced properties, Advances in Heat Transfer 16 (1984) 157–239.
[40] Z. Rouhani, E. Axelsson, Calculation of volume void fraction in a subcooled and quality region, Int. J. Heat Mass Transfer 17 (1970) 383–393.
[41] J. El Hajal, J.R. Thome, A. Cavallini, Condensation in horizontal tubes: part 2 – new heat transfer model based on flow regimes, Int. J. Heat Mass Transfer 46 (18) (2003) 3365–3387.
[42] D.C. Groeneveld, Post dry-out heat transfer at reactor operating conditions, in: ANS Topical Meeting on Water Reactor Safety, Salt Lake City, 1973.
[43] D. Gorenflo, Pool boiling (Chapter Ha)VDI Heat Atlas, VDI-Verlag, Düsseldorf, 1993.
[44] J.C. Chen, Correlation for boiling heat-transfer to saturated fluids in convective flow, Ind. Chem. Eng. Proc. Des. Dev. 5 (1966) 322–339.
[45] K.E. Gungor, R.H.S. Winterton, A general correlation for flow boiling in tubes and annuli, Int. J. Heat Mass Transfer 29 (1986) 351–358.